NOTATION

a, vibration amplitude; f, vibration frequency; f_{det}, bubble formation frequency; $\bar{f}_{det}$, mean bubble formation frequency; m_2, dispersion; x, initial first-order moment; S, mean quadratic deviation; σ, measurement error; T_s, heater surface temperature; τ, time.

LITERATURE CITED

1. W. F. Calus and P. Rice, Intern. Heat Transfer, V. S. 4, 1. Boiling (1970).
2. Schmidt and Uitt, Teploperedacha, 94, C, No. 4 (1972).
3. K. Krishia, Prasad, and V. Ramanathan, Heat Mass Transfer, 6 (1972).
4. L. D. Landau and E. M. Lifshits, Mechanics of Continuous Media [in Russian], GITTL, Moscow (1944).
5. G. F. Abezgauz et al., Handbook of Probability Calculations, No. 2 [in Russian], Voenizdat, Moscow (1970).

TWO-DIMENSIONAL RADIATIVE HEAT TRANSFER WITH ALLOWANCE FOR SHADING

V. F. Kravchenko and V. M. Yudin

UDC 536.3

Radiative heat transfer with account taken for shading in an infinite cylinder whose contour is made up of arbitrary straight-line segments and which has variable temperature and emissivity on its two sides is examined.

Calculation of heating of high-speed aircraft structures reduces to solving problems of conductive and radiative heat transfer in complex systems of thin-walled elements with internal closed spaces. Because of the peculiarities of the structure geometry and the specific heating conditions it is possible in many cases to limit examination to problems of radiative heat transfer and heat conduction in a simple configuration.

We consider radiative transfer in an infinite cylinder in which the temperature and the optical properties of the internal surface, which is assumed to be gray and diffuse, do not vary in the axial direction. We consider the cylinder to be closed; an open cylinder can be closed in many cases by introducing a fictitious surface with emissivity $\varepsilon = 1$ and temperature $T = (q_\infty/\sigma)^{1/4}$, where q_∞ is the heat flux scattered from the surrounding medium.

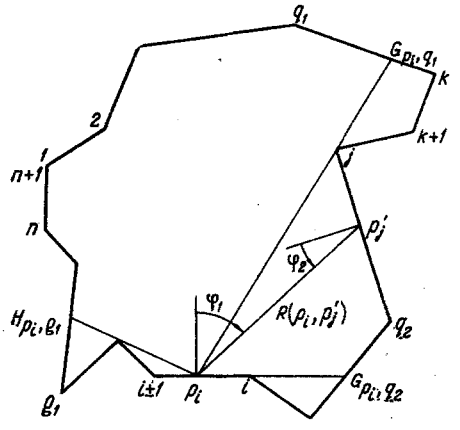

Fig. 1. Computational scheme.

N. E. Zhukovskii Central Aero-Hydrodynamics Institute, Moscow. Translated from Inzhenerno-Fizicheskii Zhurnal, Vol. 30, No. 1, pp. 49-57, January, 1976. Original article submitted January 20, 1975.

We assume that the contour of the cylinder cross section is made up of straight-line segments. This assumption corresponds to most actual problems and, in addition, any continuous contour can always be approximated by a series of straight-line segments. The temperature and emissivity vary on the two sides of the contour.

We first consider the case where the contour is nonconcave. The radiative transfer in this kind of contour is described by an integral Fredholm equation of the second kind for the incident flux density:

$$q_{\text{inc}}(p) = \oint_L \{\sigma\varepsilon(p')\,T^4(p') + [1-\varepsilon(p')]\,q_{\text{inc}}(p')\}\,K(p,\ p')\,dl', \tag{1}$$

where K(p, p') is a function of the angular coefficients,

$$K(p,\ p') = K(p',\ p) = \frac{\cos\varphi_1(p,\ p')\cos\varphi_2(p,\ p')}{2R(p,\ p')}, \tag{2}$$

and φ_1, φ_2 are the angles between the normals to the contour and the segment joining the points p and p' of length R(p, p') (see Fig. 1).

A zonal method [1-3] is widely used to solve Eq. (1). However, because the temperature varies considerably around the contours typical of aircraft structures, in using the zonal method one has to break up the contour into a large number of zones and, consequently, to solve a system of linear algebraic equations of high order. The generalized zonal method [4, 5] allows one to reduce the number of zones and thus the order of the system of algebraic equations to be solved. However, in calculating the radiative transfer in concave regions difficulties arise in allowing for shading. These difficulties can be overcome by using a quadrature method, in which the integral equation is rendered algebraic by approximating the integral with quadrature formulas. Then to increase the accuracy of the approximation it is desirable to use quadratures of very high algebraic accuracy [6]. This approach for solution of integral equations gives very good results if the kernel of the equation has no singularities. In the case considered the kernel K(p, p') has singularities at the vertices of the contour. To avoid these singularities we write Eq. (1) as the following system of integral equations for each side:

$$q_{\text{inc}}(p_i) = \sum_{j=1}^{n}\int_0^{L_j}\{\sigma\varepsilon(p_j')\,T^4(p_j') + [1-\varepsilon(p_j')]\,q_{\text{inc}}(p_j')\}\,K(p_i,\ p_j')\,dl', \tag{3}$$
$$i = 1,\ 2,\ \ldots,\ n,$$

where p_i, p_j are points on the i-th and j-th sides of the contour. Now the singularities are localized at the edges of the integration intervals and they can be avoided by integrating by parts in Eq. (3):

$$q_{\text{inc}}(p_i) = \sum_{j=1}^{n}\{\sigma\varepsilon(p_j')\,T^4(p_j') + [1-\varepsilon(p_j')]\,q_{\text{inc}}(p_j')\}\,\bar{K}(p_i,\ p_j')\Big|_{p_j'=0}^{L_j} -$$
$$-\sum_{j=1}^{n}\int_0^{L_j}\frac{d}{dl'}\{\sigma\varepsilon(p_j')\,T^4(p_j') + [1-\varepsilon(p_j')]\,q_{\text{inc}}(p_j')\}\,\bar{K}(p_i,\ p_j')\,dl', \tag{4}$$
$$i = 1,\ 2,\ \ldots,\ n,$$

where

$$\bar{K}(p_i,\ p_j') = \int K(p_i,\ p_j')\,dl' = \frac{1}{2}\sin\varphi_1(p_i,\ p_j'). \tag{5}$$

Since values of the integrand function enter into Eq. (4) at the ends of the intervals of integration, for the algebraic system of equations (4) we use a Markov quadrature formula, which includes the boundary points and has accuracy of order 2m − 3, where m is the number of nodes of integration,

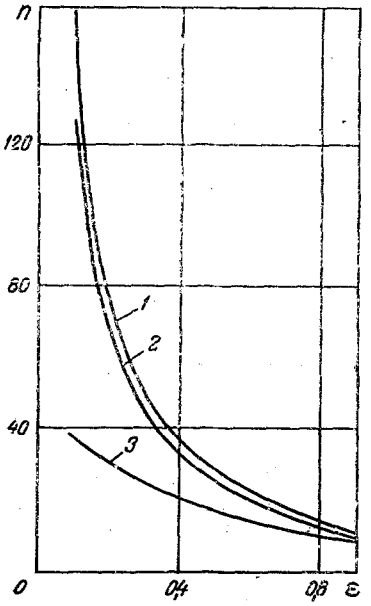

Fig. 2. Number of iterations as a function of ε: 1) simple iteration method; 2) Aitken δ^2-process; 3) using Eq. (11).

$$\int_0^L f(l)\,dl = L\int_0^1 f(\bar{l})\,d\bar{l} = L\sum_{r=1}^{m} C_r^{(m)} f(M_r^{(m)}). \tag{6}$$

The integration node coordinates $M_r^{(m)}$ and the values of the coefficients $C_r^{(m)}$ have been given in [6] up to m = 18 for the interval (−1, 1).

We use the notation

$$f(p) = \sigma\varepsilon(p)\,T^4(p) + [1-\varepsilon(p)]\,q_{\text{inc}}(p),$$

and we denote by $M_{j,k}$ and $C_{j,k}$ the Markovian integration nodes and the coefficients for the j-th side of the contour. Then the system of algebraic equations approximating the system of integral equations (4) is written in the form

$$q_{\text{inc}}(M_{i,k}) = \sum_{j=1}^{n}\{f(M_{j,m})\,\bar{K}(M_{i,k}, M_{j,m}) - f(M_{j,1})\,\bar{K}(M_{i,k}, M_{j,1})\} - \sum_{j=1}^{n}\sum_{r=1}^{m_j} C_{j,r}\,\bar{K}(M_{i,k}, M_{j,r})\,\frac{df}{d\bar{l}}(M_{j,r}), \tag{7}$$

$$i = 1, 2, \ldots, n, \quad k = 1, 2, \ldots, m_i.$$

The derivatives $df/d\bar{l}$ for both the internal and the boundary points are evaluated from values of the function f(p) at the three points:

$$\begin{aligned}
\frac{df}{d\bar{l}}(M_{j,1}) &= A_1^{(m)} f(M_{j,1}) + A_2^{(m)} f(M_{j,2}) + A_3^{(m)} f(M_{j,3}),\\
\frac{df}{d\bar{l}}(M_{j,r}) &= B_{r-1}^{(m)} f(M_{j,r-1}) + B_r^{(m)} f(M_{j,r}) + B_{r+1}^{(m)} f(M_{j,r+1}),\\
&\qquad r = 2, 3, \ldots, m-1,\\
\frac{df}{d\bar{l}}(M_{j,m}) &= D_1^{(m)} f(M_{j,m-2}) + D_2^{(m)} f(M_{j,m-1}) + D_3^{(m)} f(M_{j,m}).
\end{aligned} \tag{8}$$

In the case m = 2

$$\frac{df}{d\bar{l}}(M_{j,1}) = \frac{df}{d\bar{l}}(M_{j,2}) = f(M_{j,2}) - f(M_{j,1}). \tag{9}$$

Thus, we have obtained a system $\sum_{i=1}^{n} m_i$ of algebraic equations (7) for the incident thermal flux at the Markovian points.

To solve this system for unsteady conductive and radiative heating it is desirable to use iterative methods, since the use of the solution obtained at the (n — 1)-th step as an initial approximation at the n-th time step ensures rapid convergence of the iterative process.

In order to compare the efficiency of different iterative processes and to choose the best one, we considered the problem of radiative transfer in an irregular tetragonal region in which three sides have constant and different temperatures, and the fourth has variable temperature. The emissivities were taken to be constant and identical for all the sides. The total number of Markov points was chosen to be 20. The initial approximation was taken as zero. The iterative process was considered to end when the maximum relative difference was no more than $\Delta = 10^{-8}$.

The result was that the simple iterative method gave a more rapid divergence than the Zeidel method. With $\varepsilon = 0.5$ in the first case the number of iterations was 29, and 36 in the second case. Acceleration of convergence using the Aitken δ^2-process reduced the number of cycles in calculating q_{inc} to 26. To accelerate the convergence even more we use the condition that energy is conserved in radiative transfer in a closed cavity

$$\oint_L \varepsilon(p)\, q_{\text{inc}}(p)\, dl = \oint_L \sigma\varepsilon(p)\, T^4(p)\, dl. \tag{10}$$

Here the simple iteration algorithm was modified so that the original data for the k-th approximation, instead of the values $q_{inc}^{(k-1)}(M_{i,r})$, used the quantities

$$q_{\text{inc}}(M_{i,r}) = q_{\text{inc}}^{(k-1)}(M_{i,r}) + \theta, \tag{11}$$
$$i = 1, 2, \ldots, n, \quad r = 1, 2, \ldots, m_i,$$

where

$$\theta = \frac{\sum_{i=1}^{n} L_i \sum_{r=1}^{m_i} C_{i,r}\sigma\varepsilon(M_{i,r})\, T^4(M_{i,r}) - \sum_{i=1}^{n} L_i \sum_{r=1}^{m_i} C_{i,r}\varepsilon(M_{i,r})\, q_{\text{inc}}^{(k-1)}(M_{i,r})}{\sum_{i=1}^{n} L_i \sum_{r=1}^{m_i} C_{i,r}\varepsilon(M_{i,r})}.$$

The use of relation (11) gives substantial acceleration of convergence, particularly at small ε. Figure 2 shows data on the number of iterations for various ε, obtained from calculations using the simple iteration method (curve 1), the Aitken δ^2-process (curve 2), and Eq. (11) (curve 3).

Then after determining the incident fluxes at the Markov points the quantity q_{inc} can be obtained at any point of the contour by interpolation or by the formula

$$q_{\text{inc}}(M_s) = \sum_{j=1}^{n} \{f(M_{j,m})\,\overline{K}(M_s, M_{j,m}) - f(M_{j,1})\,\overline{K}(M_s, M_{j,1})\} - \sum_{j=1}^{n} \sum_{r=1}^{m_j} C_{j,r}\,\overline{K}(M_s, M_{j,r})\,\frac{d\overline{f}}{d\overline{l}}(M_{j,r}). \tag{12}$$

The values of q_{inc} at the supplementary points M_S, obtained from Eq. (12), can also be used in the interpolation to increase the accuracy.

In order to check the accuracy of the method of solution considered we conducted computations for 4, 6, and 9 Markov points on each side of the tetragon for the case when variable temperatures are given for all the sides, and the errors are estimated according to the Runge rule. The errors turned out to be 0.054% for four points, 0.01% for six points, and 0.0009% for nine points.

We turn now to solve the problem of radiative transfer in a region with an arbitrary contour (allowing for shading). The integral equation (1) and the system of integral equations (3) remain the same, and only the kernel

$$K(p,\ p') = K(p',\ p) = \begin{cases} \dfrac{\cos\varphi_1(p,\ p')\cos\varphi_2(p,\ p')}{2R(p,\ p')} & \text{for } \varkappa = 0, \\ 0 & \text{for } \varkappa = 1 \end{cases} \tag{13}$$

changes, where κ is the visibility parameter; for $\kappa = 0$ the point p sees p', and for $\kappa = 1$ it does not see it.

The points p and p' will see each other if the angles between the normals to the surfaces on which they lie and the intercept R(p, p') joining them are less than $\pi/2$ in absolute magnitude, i.e.,

$$\cos\varphi_1(p,\ p') > 0, \quad \cos\varphi_2(p',\ p) > 0 \tag{14}$$

and the intercept R(p, p') does not intersect any side of the contour, apart from the side on which these points lie:

$$\begin{gathered} |2t_k - 1| > 1, \quad k = 1,\ 2,\ \ldots,\ n, \\ |2t'_k - 1| > 1, \quad k \neq i,\ j, \end{gathered} \tag{15}$$

where

$$\begin{aligned} t_k &= \frac{(x_k - x_p)(y_k - y_p) - (x_k - x_{k+1})(y_k - y_p)}{(x_{p'} - x_p)(y_k - y_{k+1}) - (x_k - x_{k+1})(y_{p'} - y_p)}, \\ t'_k &= \frac{(x_{p'} - x_p)(y_k - y_p) - (x_k - x_p)(y_{p'} - y_p)}{(x_{p'} - x_p)(y_k - y_{k+1}) - (x_k - x_{k+1})(y_{p'} - y_p)}. \end{aligned} \tag{16}$$

Here x_k, y_k, x_{k+1}, y_{k+1} are the vertex coordinates, x_p, y_p, $x_{p'}$, $y_{p'}$ are the coordinates of the points p and p', and i and j are the number of sides on which these points lie.

Since the integrand function in Eq. (3) may have discontinuities in some intervals of integration because of the shading and the dependent relations (13), one must define the position of the points of discontinuity in the function, in order to allow for this in eliminating singularities and in making the system of equations algebraic. The discontinuity points are boundary points between the visible and invisible sections of the contour. Because the contour is discontinuous the visible sections must necessarily include the beginning or the end of a side, or both, if there are two invisible sections on a side. The boundaries of visible regions, between the vertices, will be the points on the horizon and the points of intersection with the first visible side of rays emitted from the test point p and proceeding through visible vertices for which

$$\cos\varphi_2(M_{j-1,m},\ p) < 0 \quad j = 2,\ 3,\ \ldots,\ n+1, \tag{17}$$

or

$$\cos\varphi_2(M_{j,1},\ p) < 0, \quad j = 1,\ 2,\ \ldots,\ n. \tag{18}$$

The condition for visibility of the j-th vertex is

$$\begin{gathered} |2t_k - 1| \geqslant 1, \quad k = 1,\ 2,\ \ldots,\ n, \\ |2t'_k - 1| \geqslant 1, \quad k \neq i,\ j-1,\ j, \end{gathered} \tag{19}$$

where t_k and t_k' are determined from Eq. (16), with $x_{p'}$ and $y_{p'}$ replaced by x_j and y_j.

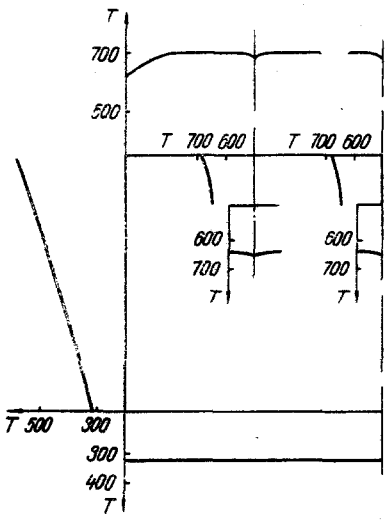

Fig. 3. Temperature distribution T (°K) over the elements of a caisson.

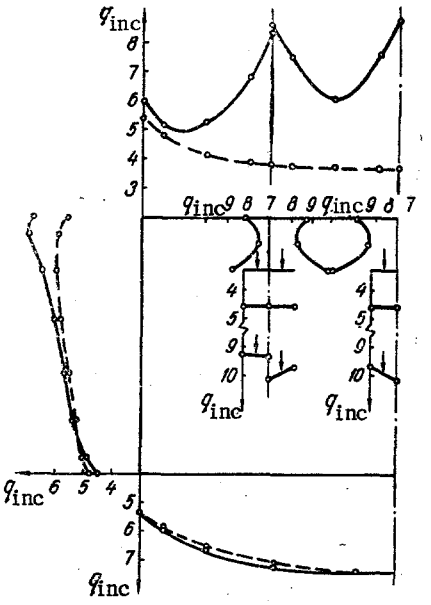

Fig. 4. Distribution of incident heat flux density q_{inc} (kW/m^2) over the internal surface of the caisson. Solid lines are with shading accounted for (with stringers); broken lines are for no shading (and no stringers).

If we add the vertices of the i-th side on which the point p lies to the visible group, then conditions (17) and (18) determine all the rays which divide the visible region from the invisible. Then rays corresponding to condition (18) determine the beginnings of the visible region, and condition (17) determines their ends.

Let $r(r_1, r_2, \ldots, r_\xi, \ldots)$, $s(s_1, s_2, \ldots, s_\tau, \ldots)$, $d(d_1, d_2, \ldots, d_\eta, \ldots)$ be, respectively, sequences of increasing numbers of all the visible vertices and vertices corresponding to conditions (17) and (18).

Then the number of sides g_η on which the point of intersection H_{p_i,g_η} corresponding to the start of a visible region, of the ray proceeding via vertex d_η, will be equal to

$$g_\eta = k \tag{20}$$

when we satisfy the conditions

$$\begin{gathered} 0 \leqslant t'_{p_i,k} < 1, \quad t_{p_i,k} = \min, \\ \cos\varphi_2(H_{p_i,k},\ p_i) > 0, \\ k = d_\eta + 1, \quad d_\eta + 2, \ \ldots\ , \ r_\xi - 1, \quad r_\xi > d_\eta = r_{\xi-1}. \end{gathered} \tag{21}$$

Similarly, for the end boundary point G_{p_i,q_τ}, corresponding to vertex s_τ, we have

$$q_\tau = k \tag{22}$$

with

$$\begin{gathered} 0 < t'_{p_i,k} \leqslant 1, \quad t_{p_i,k} = \min, \\ \cos\varphi_2(G_{p_i,k},\ p_i) > 0, \\ k = r_\xi,\ r_\xi + 1, \ \ldots\ , \ s_\tau - 1, \quad r_\xi < s_\tau = r_{\xi+1}. \end{gathered} \tag{23}$$

Here $t_{p_i,k}$ and $t_{p_i,k}'$ are calculated from Eq. (16) with x_p and y_p replaced by x_{p_i}, y_{p_i} and $x_{p'}$, $y_{p'}$ replaced by x_{d_η}, y_{d_η}, and x_{s_τ}, y_{s_τ}, respectively. The values t_{p_i,g_η}' and t_{p_i,q_τ}' obtained when conditions (21) and (23) are satisfied determine the position of the points H_{p_i,g_η} and G_{p_i,q_τ} relative to the origin of the corresponding side.

Knowing the position of the boundaries of visible regions, we can proceed to regularize and solve the system of equations (3), allowing for shading. First, for the regions of integration within which lie the corresponding boundaries of the visible regions, the lower, upper, or both limits of integration must be replaced, respectively, by the quantities t'_{p_i,g_η} and t'_{p_i,q_τ}, which determine the positions of the boundaries, and the kernel (5) is represented in the form

$$\overline{K}(p_i,\ p_j') = \begin{cases} \dfrac{1}{2}\sin\varphi_i(p_i,\ p_j') & \text{for } \varkappa = 0. \\ 0 & \text{for } \varkappa = 1. \end{cases} \tag{24}$$

When system (3) is rendered algebraic, the nodal integration points remain unchanged, but the values of the functions at points $M_{g_\eta,\,i}$ and $M_{q_\tau,m}$, under the sign of the first sum in Eq. (7), are replaced by their values at the appropriate boundary points H_{p_i,g_η} and G_{p_i,q_τ}. In the second sum the values of the functions at the points H_{p_i,g_η} and G_{p_i,q_τ} are taken instead of values of the functions at the invisible Markov points $M_{g_\eta,\gamma}$ and $M_{q_\tau,\rho}$ closest to the boundaries of the visible region and, correspondingly, are replaced by values of the coefficients

$$\begin{aligned} C_{g_\eta,\gamma} &= \sum_{k=1}^{\gamma} C_{g_\eta,k} - t'_{p_i,g_\eta}, \\ C_{q_\tau,\rho} &= \sum_{k=\rho}^{m} C_{q_\tau,k} - (1 - t'_{p_i,q_\tau}). \end{aligned} \tag{25}$$

A Fortran program was written to carry out these operations. The program computed radiative heat transfer in regions with an arbitrary contour made up of linear segments for maximum number of Markov points $\sum_{j=1}^{n} m_j = 100$ and number of sides n = 50.

This program was used to calculate radiative heat transfer in a rectangular caisson with a top three-stringer panel, with the temperature distribution of Fig. 3, typical of aircraft structures. For symmetry reasons, Fig. 3 only shows the left half of the segment. The emissivity was assumed constant over the entire contour and equal to $\varepsilon = 0.5$. The total number of Markov subdivision points was $\sum_{j=1}^{n} m_j = 85$. The position and number of these points on both sides are shown by points on the incident heat-flux-density-distribution curve shown in Fig. 4. The number of iterations for a zero initial approximation and $\Delta = 10^{-7}$ was 15. Here the distribution q_{inc} with no stringers (no shading) is shown by broken lines.

NOTATION

x,y, coordinates; l, contour coordinate; T, temperature; q_∞, heat flux from surrounding medium; q_{inc}, incident heat flux; σ, Stefan–Boltzmann constant; ε, emissivity; K(p, p'), function of angular coefficients; φ, angle; p, p', contour points; n, number of sides of the contour; L_j, length of the j-th side of the contour; m_j, number of Markov points on the j-th side; $M_{i,k}$, Markov points; $C_{i,k}$, Markov coefficients; M_S, supplementary points; A, B, D, coefficients; κ, visibility parameters; t_k, t_k', parameters; $H_{p_i,\,g_\eta}$, initial point of the visible region; $G_{p_i,\,q_\tau}$, final point of a visible region; $t'_{p_j,\,k}$, relative distance of boundaries of the visible region from the beginning of the side; Δ, maximum relative error.

final point of a visible region; G_{p_i,q_τ}, final point of a visible region; $t'_{p_i,k}$, relative distance of boundaries of the visible region from the beginning of the side; Δ, maximum relative error.

LITERATURE CITED

1. L. G. Polyak, Zh. Tekh. Fiz., 5, No. 3 (1935).
2. Yu. A. Surinov, Izv. Akad. Nauk SSSR, Otd. Tekh. Nauk, No. 9 (1950).
3. G. N. Zamula and V. M. Marchenko, in: Thermal Stresses in Structural Elements, No. 5 [in Russian], Kiev (1965).
4. V. N. Andrianov, Fundamentals of Radiative and Combined Heat Transfer [in Russian], Energiya, Moscow (1972).
5. V. M. Yudin, Uch. Zap. Tsentr. Aéro-Gidrodinam. Inst., 5, No. 3 (1974).
6. V. I. Krylov, Approximate Evaluation of Integrals [in Russian], Nauka, Moscow (1967).

RADIATION OF SULFUR DIOXIDE

Yu. A. Popov

UDC 536.3

Using spectral-analysis data and the statistical model of Goody, the emissivity and absorption coefficient of sulfur dioxide are calculated.

In many furnaces of nonferrous metallurgy and the chemical industry it is required to make allowance for the radiation of sulfur dioxide, SO_2. The nomograms of the integrated emissivity ε_{SO_2} presented in [1] were based on the Bouger law, which is not satisfied for the vibrational–rotational absorption bands of a gas when the frequency-averaging interval exceeds the width of the spectral lines. The calculation presented in [2] was based on the Edwards band contour model, which fails to describe the contour of the vibrational–rotational bands accurately enough. Reliable results for the integrated emissivity of SO_2 were obtained experimentally by Golitsin and Berlin [3, 4]. These results lay roughly 40% below those of [1] and were approximately double the theoretical data of Chan and Tien [2]. However, the volume of experimental material in [3, 4] was insufficient for practical application, and the empirical formulas proposed in [3] are insufficiently accurate even in the region covered by the experiments (Fig. 2).

In this paper we shall calculate the integrated emissivity and absorption coefficient of SO_2 using the statistical model of the absorption bands of gases developed by Goody [8]. In order to choose the parameters of the model and the shape of the band contour we used the spectral results obtained at room temperature by Chan and Tien [2]. An analogous method was employed for calculating the emissivity and absorption coefficient of CO_2 and water vapor [5].

The SO_2 molecule is nonlinear; its rotational constants are well known [6]:

$$A=2.027\ \text{cm}^{-1};\quad B=0.3442\ \text{cm}^{-1};\quad C=0.2935\ \text{cm}^{-1}.$$

The smoothed absorption coefficient of the band i of a nonlinear molecule takes the form [5]

$$\tilde{k}_{\nu i}=k_{0i}P_0\frac{x_i(1-e^{-x})}{\sqrt{T}\,Q_i(T)}\,|y_i|\exp[-\gamma T y_i^2 f_i(y_i T)]. \qquad (1)$$

Here $x_i = hc\nu_i/kT$, $x = hc\nu/kT$, $y_i = x_i - x$. The constant γ is determined by the expression

All-Union Scientific-Research Institute of Metallurgical Heat Technology, Sverdlovsk.

Translated from Inzhenerno-Fizicheskii Zhurnal, Vol. 30, No. 1, pp. 58-62, January, 1976. Original article submitted December 20, 1974.